# Hybrid Organic/Inorganic Interphase for Stabilizing a Zinc Metal Anode in a Mild Aqueous Electrolyte

Huifang Fei, Jin Han, Stefano Passerini,* and Alberto Varzi*

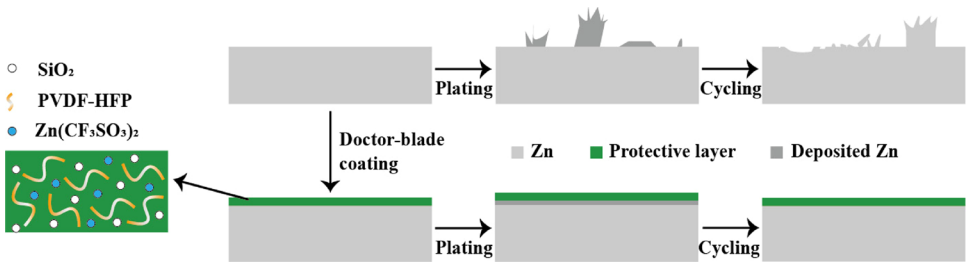


**ABSTRACT:** Aqueous rechargeable zinc-based batteries have recently gained tremendous attention because of their low cost and high safety. However, the issues associated with the zinc metal anode, including corrosion, $H_2$ evolution, and dendrite growth, hinder their practical applications. Herein, we design a hybrid organic/inorganic interphase composed of poly(vinylidene fluoride-co-hexafluoropropylene), silica, and zinc triflate to stabilize the zinc metal anode in a mild aqueous electrolyte. It is proven that the artificial interphase reduces corrosion of the Zn metal in the $ZnSO_4$ electrolyte and suppresses dendrite growth by regulating $Zn^{2+}$ deposition. Therefore, the lifespan of symmetrical cells with coated Zn could be enhanced to over 960 h with a stripping/plating capacity of 0.5 mAh $cm^{-2}$. In addition, zinc-ion batteries including a sodium vanadate cathode and a coated Zn anode could achieve 3000 cycles with nearly no capacity fading at 5 A $g^{-1}$.

**KEYWORDS:** *zinc metal anode, PVDF-HFP, silica, sodium vanadate, interphase engineering, mild aqueous electrolyte*

## INTRODUCTION

A promising strategy for replacing traditional fossil fuels as an energy source is to efficiently exploit renewable and clean energy from wind, water, sunlight, and tides by implementing energy storage systems (ESSs).[1] Rechargeable batteries, in particular lithium-ion batteries (LIBs), are among the most intensively studied storage devices for ESSs.[2] Although LIBs with organic electrolytes possess high energy density, excellent cycling stability, and suitability for application in electrical vehicles and portable electronic devices, alternative chemistries with improved environmental benignity, higher safety, and lower cost are needed for grid-scale ESS applications.[3,4] Rechargeable aqueous batteries with sustainable and abundant electrode materials are particularly promising systems.[4] Among them, zinc-based systems such as zinc-ion batteries (ZIBs) have recently attracted tremendous attention because of the high theoretical capacity (820 mAh $g^{-1}$), low electrochemical redox potential, and low cost of Zn.[5−7] Additionally, neutral electrolytes, instead of the traditional alkaline solutions, enable rechargeable ZIBs.[8] Although great progress has been made with regard to $Zn^{2+}$ insertion materials, multiple issues at the zinc metal anode still hinder the practical application of ZIBs. The growth of zinc dendrites and the spontaneous reaction with the aqueous electrolyte remain the main obstacles to achieve long cycle life in ZIBs.[9,10] On the one hand, the uneven Zn deposition causes dendrite growth and dead Zn, resulting in cell failure by short circuit and poor reversibility. On the other hand, Zn spontaneously reacts with the aqueous electrolyte, leading to the formation of inert byproducts and consuming both Zn and the electrolyte. These processes, including the undesirable hydrogen evolution, substantially reduce the Coulombic efficiency (CE) of ZIBs.[8]

Many effective strategies were proposed to enable uniform Zn deposition and inhibit side reactions,[11,12] such as designing a Zn micromesh to induce spatial-selection deposition,[13] modifying the electrolyte with a cosolvent to change the solvation structure and form a beneficial solid interface,[14] and constructing electrode−electrolyte interphases to protect zinc from parasitic reactions and regulate $Zn^{2+}$ deposition.[15−17]

Among them, fabricating a protective layer is one of the most effective, simple, and direct methods to prevent Zn from directly contacting the electrolyte and possibly regulate Zn deposition.[16] Many approaches toward the design of artificial

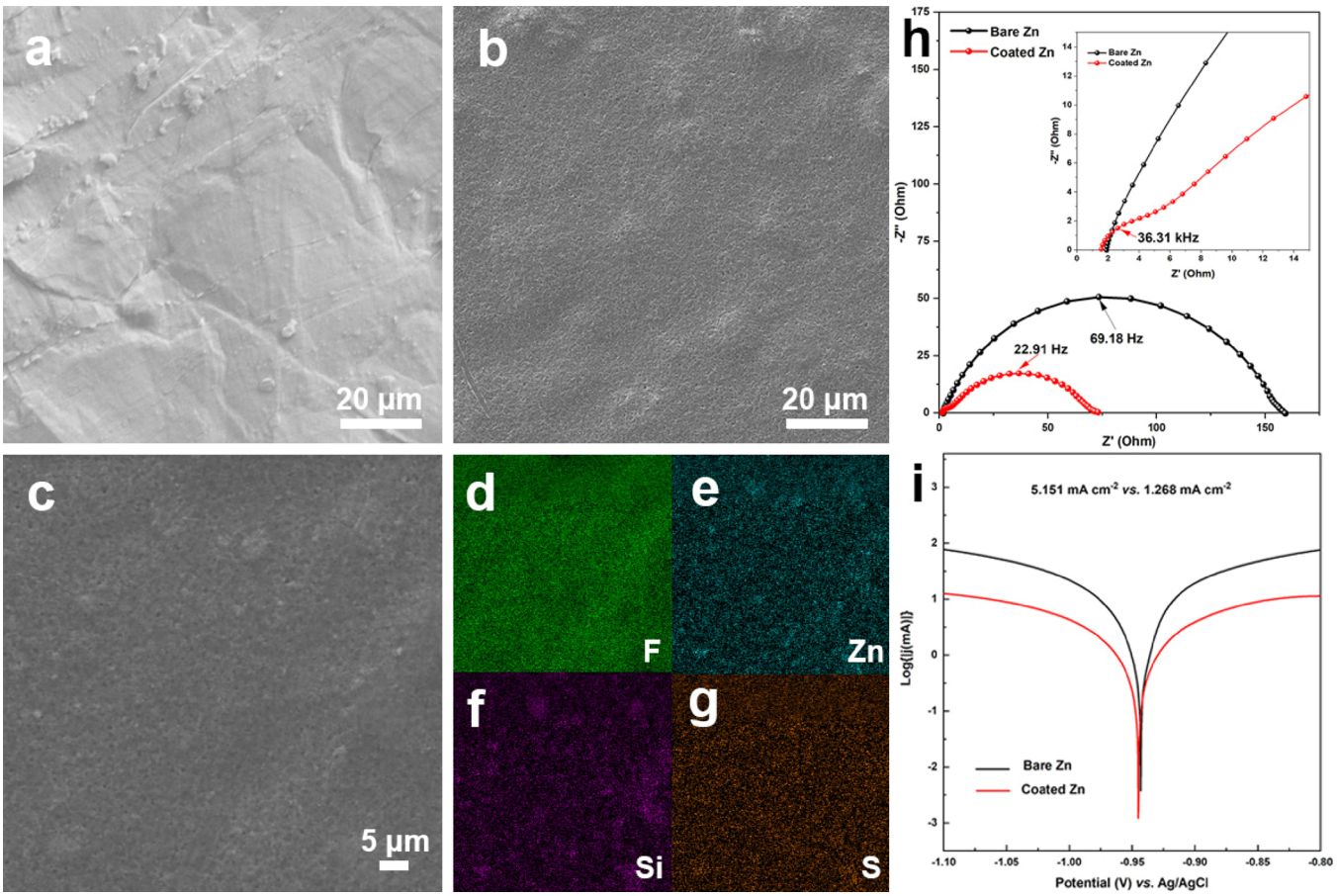


**Figure 1.** SEM images of (a) bare and (b) coated Zn foils. (c–g) SEM image of a coated Zn foil with corresponding EDX mapping images. (h) Nyquist plot of symmetrical Zn/Zn cells employing bare or coated Zn electrodes in a 2 M $ZnSO_4$ electrolyte. The inset highlights the high-frequency features. (i) Linear polarization (Tafel) curves of bare and coated Zn electrodes. In these last measurements, a Zn foil was used as the counter electrode and a leakless Ag/AgCl electrode was used as the reference electrode. The electrolyte was 2 M $ZnSO_4$ (aqueous) and the scan rate was 5 mV $s^{-1}$.

interphases were developed to inhibit anode corrosion and to modify the Zn surface by adjusting the current distribution. Among them, artificial interphases containing oxide coatings, polymeric films, and organic–inorganic hybrid protection layers were proposed.[18,19] In particular, polyvinylidene fluoride (PVDF)-based coating matrixes, such as PVDF-MOF[20] and PVDF-$TiO_2$,[21] can overcome the shortcomings of fully inorganic layers (i.e., brittleness). Additionally, a poly(vinylidene fluoride-co-hexafluoropropylene) (PVDF-HFP) layer with dissolved Zn salt possesses high ionic conductivity and low crystallinity and can be utilized as a polymer host for gel electrolytes and all-solid-state electrolytes in ZIB.[22,23] In addition, PVDF-HFP can be easily shaped into uniform thin films, which will only slightly sacrifice the overall energy density of the resulting battery.[15]

In this study, we design a PVDF-HFP-based coating layer including zinc triflate and silica to regulate Zn deposition and reduce interfacial resistance between the zinc anode and a mild $ZnSO_4$ aqueous electrolyte. PVDF-HFP is intrinsically hydrophobic, but with the addition of zinc triflate ($Zn(OTf)_2$) and hydrophilic silica, the layer exhibits better interfacial performance with the zinc sulfate electrolyte compared to an unmodified zinc surface.[16] Furthermore, this artificial interphase could regulate the Zn deposition and stabilize the cycling performance of ZIBs with a $NaV_3O_8{\cdot}1.5H_2O$ (NVO) cathode and a coated Zn anode. Symmetrical cells with coated Zn electrodes also show much longer cycling performance than those with the bare Zn, with a fixed stripping/plating capacity of 0.5 mAh $cm^{-2}$.

## RESULTS AND DISCUSSION

Scanning electron microscopy (SEM) images were recorded to investigate the morphology of bare (Figure 1a) and coated (Figure 1b) Zn foils. The comparison of the SEM images reveals that the Zn surface is effectively covered by a uniform composite layer. The energy-dispersive X-ray (EDX) mapping of the coated Zn sample (Figure 1c–g) reveals the rather homogeneous distribution of Zn and S signals arising from zinc triflate and Si from silica confirming the uniformity of the coating layer. The thickness of the coating was determined to be ca. 3.5 $\mu$m by the cross-sectional SEM images recorded after focused ion beam (FIB) milling. The coating layer is quite uniform as well (Figure S1). Efforts to reduce the thickness of the layer using our doctor blade equipment were unsuccessful, resulting in rather inhomogeneous coatings. Further approaches (e.g., spray- or spin-coating) are currently being developed and will be a subject of a future study. X-ray diffraction (XRD) characterizations were performed to further reveal the structure of the protective layer (Figure S2). Fumed silica shows no featured peaks due to its highly amorphous structure, while the pattern of zinc triflate matches well with that of the standard PDF 01-075-4449. The two characteristic

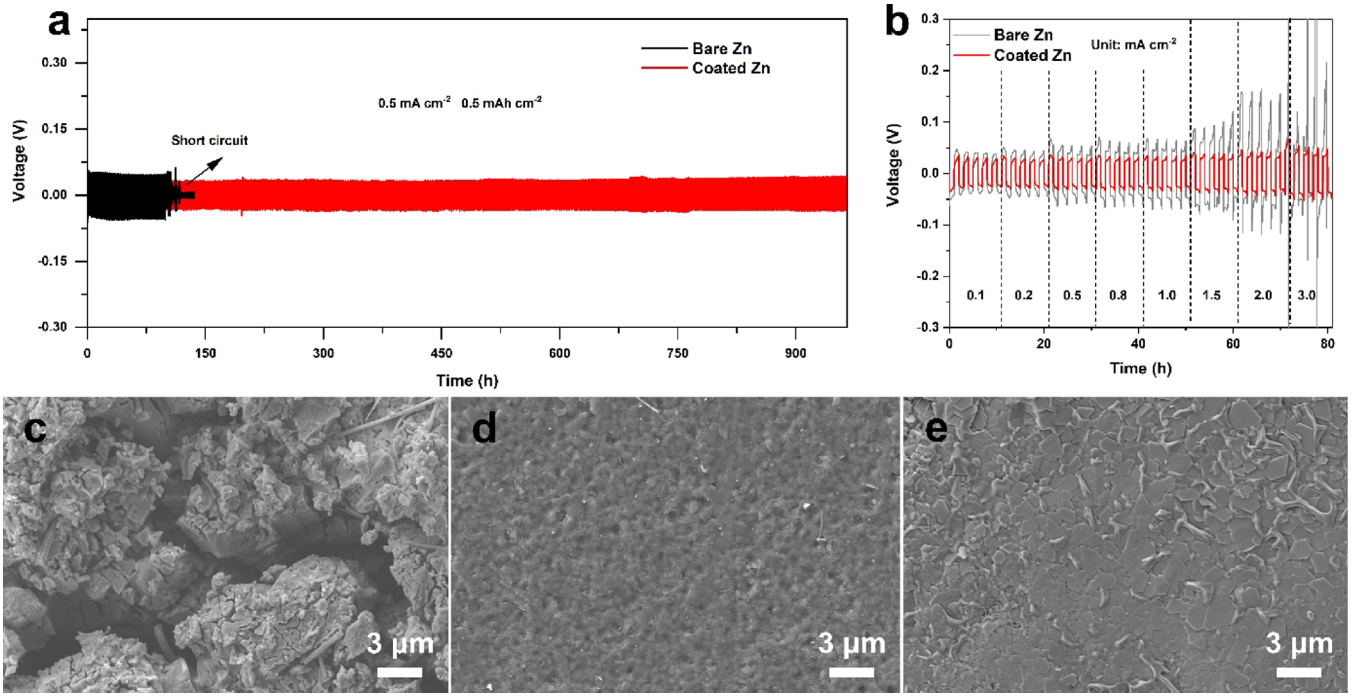


**Figure 2.** (a) Long-term galvanostatic stripping/plating tests of symmetric Zn cells with bare or coated Zn electrodes at a current density of 0.5 mA $cm^{-2}$ (1 h for each step). (b) Stripping/plating voltage of symmetric Zn cells at different current densities. SEM images of bare (c) and coated (d) Zn electrodes disassembled from symmetrical cells after 10 cycles. (e) SEM image of the coated Zn (disassembled from symmetrical cells after 10 cycles) after removal of the protection layer. All measurements were performed in a 2 M $ZnSO_4$ electrolyte.

peaks of the pure PVDF-HFP membrane are located at 18.1 and 20.0°, in agreement with the previous literature.[24] After the addition of silica and zinc triflate into PVDF-HFP, the characteristic diffraction peaks of the highly crystalline $Zn(OTf)_2$ disappeared as shown by the XRD pattern of the protective layer, indicating that the salt is completely dissolved into the PVDF-HFP polymer matrix. The XRD pattern of the coated Zn corresponds well with that of the protective layer, with additional features characteristic of metallic Zn. In addition, two unassigned peaks located at 29.9 and 40.0° appear both on the protective layer and on the coated Zn. Their nature is yet unknown; however, it could be speculated that they arise from some kind of crystalline structure including residual DMF solvent.

To understand the role of each component of the protective layer, three types of coating (neat PVDF-HFP, PVDF-HFP/silica, and PVDF-HFP/triflate) were applied on the Zn anode and control experiments were performed (Figure S3). As Figure S3a shows, the symmetrical cell with PVDF-HFP-coated Zn electrodes displays quite large voltage polarization, indicating that the pure PVDF-HFP coating layer is ion-blocking. The addition of silica does not lead to any noticeable improvement (Figure S3b). On the other hand, the symmetrical cell with PVDF-HFP/$Zn(OTf)_2$-coated Zn displays comparatively small polarization. Nevertheless, the cell soon experiences short circuit, as evidenced by the voltage profiles (Figure S3c). These control experiments clearly demonstrate that the presence of Zn triflate is fundamental to provide ionic conduction through the protective layer, while silica ensures long-term cycling by suppressing the dendrite growth.

To determine the influence of the coating layer on the electrochemical properties of the Zn foil, symmetrical Zn/Zn cells were assembled and characterized by electrochemical impedance spectroscopy (EIS). The Nyquist plot in Figure 1h shows a slightly different response for the two systems, with a small additional semicircle present at a high frequency for the cell employing coated Zn electrodes. This can be attributed to the artificial interphase (coating), however featuring a very low impedance (8.8 Ω). In addition, the charge-transfer resistance of the cell with coated Zn electrodes (68.5 Ω) is lower than that of the cell with bare Zn electrodes (146.2 Ω). In fact, the poor wetting of the pristine Zn surface by the aqueous electrolyte results in increased interfacial free energy contributing to a large interfacial resistance and uneven Zn electrodeposition.[25] In fact, the overall interfacial resistance is effectively reduced by the addition of the coating layer, suggesting that the zinc triflate and silica in the hybrid, PVDF-HFP-based protection layer offer a more compatible surface for homogenous Zn-ion transport. Furthermore, the corrosion current measured for bare and coated Zn electrodes is 5.151 and 1.268 mA $cm^{-2}$, respectively (see Figure 1i). This suggests that the coating layer efficiently suppresses corrosion of Zn in the 2 M $ZnSO_4$ electrolyte.[26] It should be mentioned that all symmetric cells with bare Zn opened up during cycling, while those with coated Zn remained sealed without any evident swelling for hundreds of cycles. This evidence confirms that the protection layer could suppress $H_2$ evolution. In addition, bond strength tests were conducted to verify the adhesive property of the protective layer to Zn. The adhesion strength is 0.9324 N $mm^{-2}$ (932.4 kPa) with a standard deviation of 0.2507 N $mm^{-2}$. Such a value is in line with the previous literature and even higher than the adhesion strength (51 kPa) of PVDF-based activated carbon electrodes previously developed by our group for capacitor applications.[27]

To further investigate the electrochemical performance of symmetrical cells and the morphological evolution of Zn deposition, stripping/plating tests under different conditions were conducted. The long-term cycling and rate performance

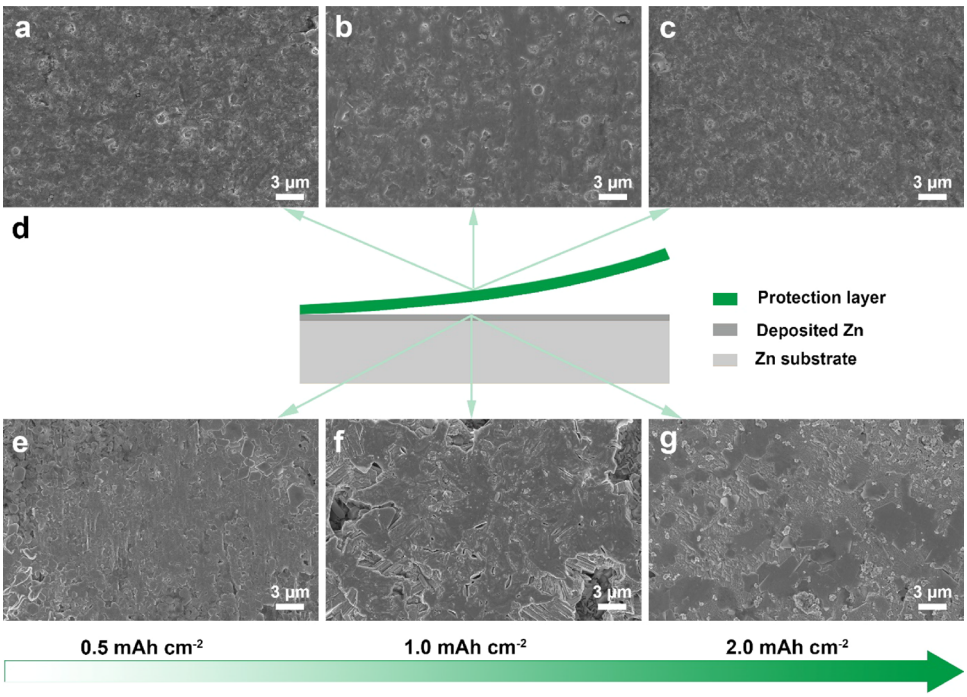


**Figure 3.** Morphology evolution of coated Zn electrodes after deposition of different Zn amounts. (a–c) SEM images of the top surface of the coated Zn electrode after deposition with Zn at current densities of 0.5, 1.0, and 2.0 mA $cm^{-2}$ for 1 h, respectively. (d) Schematic illustration of the SEM measurement. (e–g) Corresponding SEM images of the coated Zn electrode after peeling off the protection layer with Zn deposition of 0.5, 1.0, and 2.0 mAh $cm^{-2}$, respectively.

of symmetrical cells are displayed in Figure 2a,b, respectively. Figure 2a shows the galvanostatic tests of symmetrical cells with bare or coated Zn at a current density of 0.5 mA $cm^{-2}$. The lifespan of the symmetrical cell with a bare Zn anode reaches only 106 h before signs of short circuit begin to appear. In contrast, the symmetrical cell with coated Zn electrodes displays stable voltage profiles for over 960 h with a small hysteresis of 77 mV (Figure S4) and no sign of short circuit, confirming the dendrite suppression function of silica. Afterward, the morphological changes of the electrode surface after 10 cycles were investigated. As Figure 2c shows, the unmodified Zn displays a rough and fractured surface, which may partially be attributed to the side products of corrosion confirmed by the XRD pattern of the bare Zn electrode after cycling (Figure S5).[8] By comparison, the coated Zn demonstrates nearly no morphology change compared to that before cycling (Figure 2d). Furthermore, the XRD diffractograms of coated Zn after cycling (Figure S5) prove that the protective layer can suppress Zn anode corrosion in an aqueous $ZnSO_4$ electrolyte. Interestingly, the two unassigned peaks previously observed (see Figure S2) have also disappeared. This corroborates the hypothesis of residual DMF being initially present in the artificial interphase. Being miscible in water, the solvent dissolved in the electrolyte during cycling, leading to the disappearance of the XRD peaks. After peeling off the coating layer with tweezers (Figure 2e), the Zn deposits underneath appeared flat and relatively dense, indicating that the hybrid layer is able to regulate Zn deposition and suppress dendrite growth.

Stripping/plating tests at increasing current densities were also performed to symmetrical cells (Figure 2b). As the current density increased, the cell with bare Zn always displayed larger polarization than that employing coated Zn electrodes, resulting from the larger interfacial resistance with the electrolyte. When the current density reached 3.0 mA $cm^{-2}$, the cell with bare Zn electrodes suffered from short circuit due to dendrite growth, while the one with coated Zn electrodes exhibited a stable stripping/plating behavior with a rather stable voltage hysteresis of just 100 mV.

To further investigate the influence of the coating layer during Zn deposition, 0.5, 1.0, and 2.0 mAh $cm^{-2}$ of Zn were deposited on bare or coated Zn substrates. Regarding the bare Zn electrode, inhomogeneous deposits occurred (see Figure S6), which grew through the separator, as demonstrated by the glass fibers embedded in the electrode surface, ultimately causing short circuits (see Figure 2a). After deposition of 0.5 mAh $cm^{-2}$, the SEM images (Figure S6a,b) display small protuberances on irregular and loose particles. These grew into larger flakes while the overall deposits became denser after the deposition of 1 mAh $cm^{-2}$ of Zn (Figure S6c,d). For 2.0 mAh $cm^{-2}$-deposited Zn, the electrode morphology (Figure S6e,f) is dominated by larger flakes growing in different directions. In contrast, the morphology of Zn deposited under the hybrid coating layer was relatively flat without appreciable morphological changes at high deposition capacities as it can be seen from Figure 3a–c. Figure 3d schematically depicts the SEM measurement. After removal of the coating layer, the underlying Zn deposits display uniform appearance in all cases (Figure 3e–g). The results confirm that the Zn ion can be effectively transported through the hybrid layer and deposited on the Zn electrode, probably resulting from the $Zn^{2+}$ complexation/decomplexation transport mechanism in the PVDF-HFP/$Zn(OTf)_2$ complex system.[22] Figure S7 shows the EIS characterization of the coating layer in a dry pouch cell (i.e., without any aqueous electrolyte) from which its ionic conductivity is calculated to be $3.37 \times 10^{-5}$ S $cm^{-1}$, which is in line with a previous study.[22] The resistance value obtained from the artificial interlayer shown in Figure 1h is smaller than

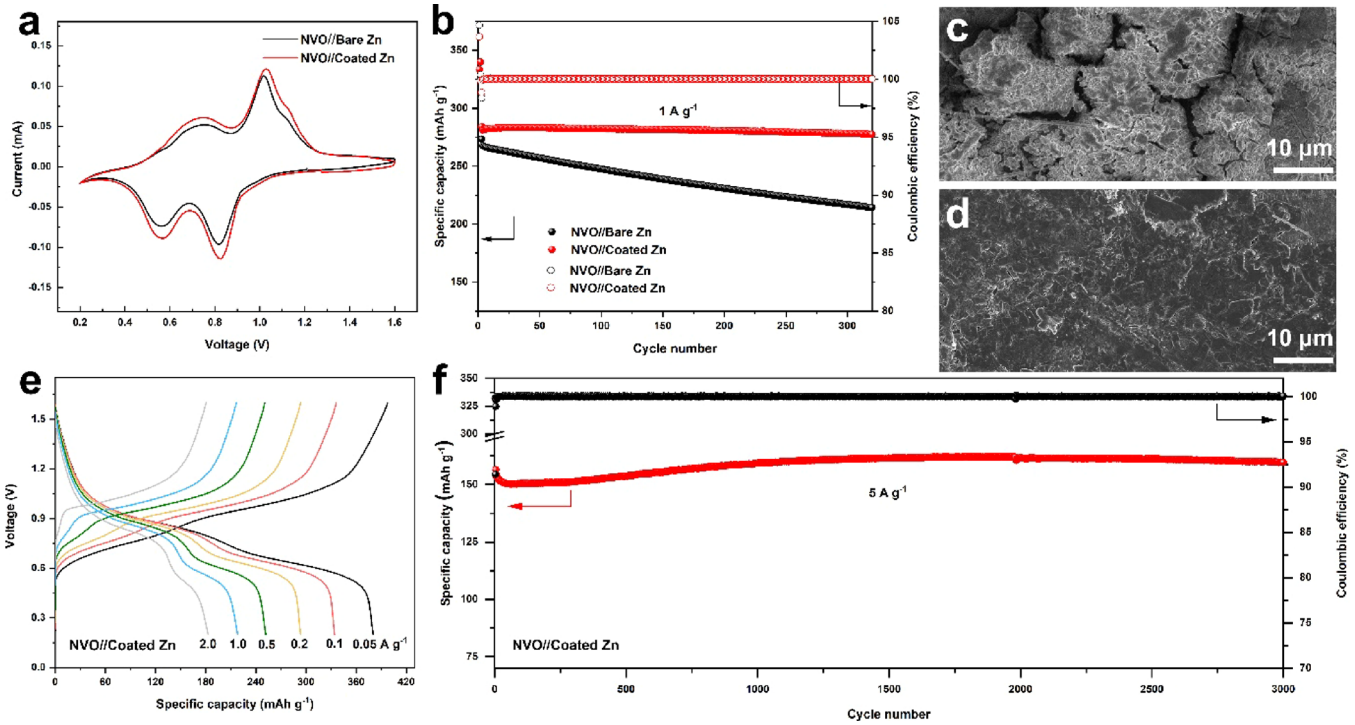


**Figure 4.** Electrochemical performance of ZIBs with an NVO cathode. (a) CV curves and (b) cycling performance at 1 A $g^{-1}$ between 0.2 and 1.6 V of NVO/Zn full ZIBs employing bare or coated Zn electrodes. SEM images of (c) bare and (d) coated Zn electrodes disassembled from ZIBs after 10 cycles. (e) Voltage profiles of an NVO/coated Zn full ZIB at various current densities. (f) Long-term cycling performance of an NVO/coated Zn full ZIB at a current density of 5 A $g^{-1}$ between 0.2 and 1.6 V.

the impedance of the dry polymer, which may be caused by the fact that the protection layer is not entirely impermeable to the aqueous solution and an excess of aqueous electrolyte in the cell may wet the edge of the Zn anode. In summary, the coating layer regulates Zn-ion transport allowing for homogeneous Zn deposition. The voltage profiles upon first plating are also displayed in Figure S8. Here, it can be noticed that the Zn nucleation overpotential on the coated Zn electrode is substantially smaller than that on bare Zn. The same coating layer was also applied to a Cu foil (Figure S9) to further investigate the influence of such a protective layer on the efficiency of Zn deposition/dissolution, as shown in Figures S10 and S11. Upon long-term cycling, the voltage polarization and CE (Figure S10) have been improved a lot for coated Cu.

To investigate the effectiveness of the hybrid coating in ZIBs, full cells with NVO as a cathode and either bare or coated Zn as an anode were assembled. Here, the concentration of the $ZnSO_4$ aqueous electrolyte was increased to 3 M to efficiently suppress the dissolution of the cathode active material.[28] The NVO cathode was synthesized according to the previous literature.[29] The XRD pattern of the powder (Figure S12a) matches that of the standard PDF 16-1601, confirming the phase purity and crystalline structure of the cathode material, which has a nanorod-type microstructure (Figure S12b). Cyclic voltammetry (CV) curves (Figure 4a) of the cells were recorded between 0.2 and 1.6 V at a scan rate of 0.05 mV $s^{-1}$. According to Wan's research, the two pairs of redox peaks located at 0.56/0.75 and 0.82/1.03 V correspond to the intercalation and deintercalation of $Zn^{2+}/H^{+}$ ions at the same time in NVO, respectively.[29] Upon long-term galvanostatic cycling at 1 A $g^{-1}$ from 0.2 to 1.6 V (Figure 4b), the capacity retention of the ZIB employing coated Zn is 96.7% after 300 cycles. However, the one with bare Zn only retains 79.3% of the initial capacity due to the continuous corrosion of the unprotected Zn anode. The SEM images after cycling provide additional evidence for the capacity fading of the ZIBs employing the bare Zn electrode. A very porous and dendritic surface with large cracks is observed on bare Zn (Figure 4c), which may be caused by the corrosion between Zn and the aqueous electrolyte. On the other hand, the surface of coated Zn appears flat after peeling off the protection layer (Figure 4d). As shown in Figure 4e, the rate capability of the NVO/coated Zn ZIB cell is reported. On increasing the current density from 0.05 to 2.0 A $g^{-1}$, the cell could deliver discharge capacities of 380, 334, 293, 252, 218, and 183 mAh $g^{-1}$. Furthermore, the cell displayed excellent stability upon cycling at high current rates as shown in Figure 4f. In fact, a discharge capacity exceeding 150 mAh $g^{-1}$ could be delivered for up to 3000 cycles at 5 A $g^{-1}$ (ca. 8.0 mA $cm^{-2}$).

## CONCLUSIONS

In conclusion, a hybrid organic/inorganic artificial interphase composed of a PVDF-HFP polymer matrix filled with fumed silica and added with Zn salt was designed and applied to Zn and Cu foils by a simple doctor blade coating method. The SEM characterization revealed the homogenous distribution of the hybrid interphase on the substrate. Zn ions can be effectively transported through the interphase by the complexation/decomplexation within the polymer segments and uniformly deposited on the Zn substrate, as confirmed by SEM images. The EIS results of the symmetrical cell with or without a protection layer and linear polarization curves demonstrate that the protection layer could effectively suppress the corrosion. The long-term cycling performance of both symmetrical and asymmetrical and full cells with coated Zn or

Cu electrodes is substantially improved compared to those employing the bare metal foils.

## EXPERIMENTAL SECTION

**Materials.** The NVO cathode was synthesized following the method previously reported by Wan's research group.[29] Typically, 1 g of $V_2O_5$ (99.6%, Alfa Aesar) was stirred in 15 mL of a NaCl (99.99%, VWR) aqueous solution (2 M) for 72 h at room temperature. Then, the resultant powder was collected by centrifugation and washed three times using water and ethanol. At last, the dark red powder was heated in an oven at 80 °C for 24 h. A Zn foil (99.95+%) with a thickness of 75 $\mu$m was bought from Goodfellow. The coated Zn foil was fabricated using the simple doctor blade method. The coating solution consists of 1.2 g of PVDF-HFP (pellets, Sigma-Aldrich), 0.4 g of zinc triflate (99%, Solvionic), and 0.12 g of silica (nanopowder with a particle size of 0.007 $\mu$m, Sigma-Aldrich) in 8 g of DMF (99.9%, Alfa Aesar). After coating the slurry (a wet thickness of 45 $\mu$m), the Zn foil was dried at 80 °C in vacuum. The same coating and drying procedure was also applied to a copper foil with a thickness of 3.5 $\mu$m (Wellcos Corporation, 99.90+%). All the electrolytes (2 and 3 M $ZnSO_4$) were homemade by dissolving appropriate amounts of zinc sulfate heptahydrate (Alfa Aesar) in high-purity water (Millipore Milli-Q).

**Characterization Methods.** The crystallographic structure of NVO was determined by a Bruker D8 Advance diffractometer. The morphology and composition investigations were carried out using a scanning electron microscope (ZEISS Crossbeam XB340) equipped with an EDX detector. To precisely determine the thickness of the protective layer, a Capella FIB (gallium ion source) was used to expose the cross section of the coated Zn with milling (30 nA) and polishing (3 nA) at an accelerating voltage of 30 kV. After FIB preparation, the micrographs were acquired from the top with a tilt angle of 54°, and smart SEM software for tilt correction was used to compensate for the image distortion due to the tilt. The bond strength test between the protective layer and Zn was conducted using a Z2.5 Zwick/Roell machine. The coated Zn (square shape with 6.45 $cm^{-2}$) was fixed to the sample holder using 3M tape (3 M Double Coated Paper Tape 410M), and to the opposite movable sample holder (vertical direction), only the tape was attached. Afterward, 2500 N of force was applied to the coated Zn for 30 s to ensure intimate contact. Finally, the protective layer was peeled off from Zn at a speed of 100 mm $min^{-1}$ and the maximum tensile strength was recorded. The tensile stress is calculated as the tensile strength to the testing surface area. Five samples were tested and the average value, including standard deviation, was calculated.

**Electrochemical Characterization.** The ionic conductivity of the dry coating layer (i.e., without the addition of any liquid electrolyte) was measured using a Solartron Analytical (Ametek) impedance analyzer 1287 with a pouch cell at a frequency of 100−$10^6$ Hz.

The symmetric cells were composed of bare or coated Zn electrodes, 100 $\mu$L of $ZnSO_4$ (2 M), and a GF/F separator (Whatman) hosted in 2032 coin cells. The stripping/plating experiments were conducted using a battery cycler (Maccor 4000). The Tafel plots of bare or coated Zn electrodes were realized using a programmable potentiostat (VMP3 BioLogic Science) and three-electrode T-cells employing a bare or coated Zn working electrode, a Zn counter electrode, and a leakless Ag/AgCl (3.4 mol $L^{-1}$ KCl, 0.224 V vs standard hydrogen electrode) reference electrode. Zn stripping/plating tests on a bare or coated Cu foil were carried out with a fixed capacity of 1.0 mAh $cm^{-2}$ at a current density of 2.0 mA $cm^{-2}$.

The NVO cathode electrodes were made by coating the slurry (70 wt % NVO, 20 wt % Super C65, and 10 wt % PVDF) on a titanium foil. The active material loading of the cathode was ca. 1.8 mg $cm^{-2}$. The cycling performance of the NVO/Zn coin cells was tested in the 0.2−1.6 V voltage range at different current densities. The electrolyte used for full ZIBs was a 3 M $ZnSO_4$ solution. The CV curves of full ZIBs were collected using a programmable potentiostat (VMP3) at a scan rate of 0.05 mV $s^{-1}$. The EIS results of the symmetrical cells were collected using a Solartron Analytical (Ametek) impedance analyzer 1287 at a frequency range of $10^6$−0.01 Hz. All the electrochemical tests were conducted at 20 °C.

## AUTHOR INFORMATION


### Corresponding Authors

**Stefano Passerini** − *Helmholtz Institute Ulm (HIU), D-89081 Ulm, Germany; Karlsruhe Institute of Technology (KIT), D-76021 Karlsruhe, Germany;* orcid.org/0000-0002-6606-5304; Email: stefano.passerini@kit.edu

**Alberto Varzi** − *Helmholtz Institute Ulm (HIU), D-89081 Ulm, Germany; Karlsruhe Institute of Technology (KIT), D-76021 Karlsruhe, Germany;* orcid.org/0000-0001-5069-0589; Email: alberto.varzi@kit.edu

### Authors

**Huifang Fei** − *Helmholtz Institute Ulm (HIU), D-89081 Ulm, Germany; Karlsruhe Institute of Technology (KIT), D-76021 Karlsruhe, Germany*

**Jin Han** − *Helmholtz Institute Ulm (HIU), D-89081 Ulm, Germany; Karlsruhe Institute of Technology (KIT), D-76021 Karlsruhe, Germany*


### Notes

The authors declare no competing financial interest.

## ACKNOWLEDGMENTS


H.F. sincerely acknowledges the financial support from the China Scholarship Council. Financial support from the Helmholtz Association is also acknowledged. We sincerely appreciate the help from Dominik Stepien for the FIB measurement and Jakob Asenbauer for the tensile strength test.

## REFERENCES


(1) Liu, C.; Li, F.; Ma, L.-P.; Cheng, H.-M. Advanced Materials for Energy Storage. *Adv. Mater.* **2010**, *22*, E28−E62.

(2) Manthiram, A.; Fu, Y.; Su, Y.-S. Challenges and Prospects of Lithium-Sulfur Batteries. *Acc. Chem. Res.* **2013**, *46*, 1125−1134.

(3) Kundu, D.; Adams, B. D.; Duffort, V.; Vajargah, S. H.; Nazar, L. F. A high-capacity and long-life aqueous rechargeable zinc battery using a metal oxide intercalation cathode. *Nat. Energy* **2016**, *1*, 16119.

(4) Tarascon, J. M.; Armand, M. Issues and challenges facing rechargeable lithium batteries. *Nature* **2001**, *414*, 359−367.

(5) Fang, G.; Zhou, J.; Pan, A.; Liang, S. Recent Advances in Aqueous Zinc-Ion Batteries. *ACS Energy Lett.* **2018**, *3*, 2480−2501.

(6) Song, M.; Tan, H.; Chao, D.; Fan, H. J. Recent Advances in Zn-Ion Batteries. *Adv. Funct. Mater.* **2018**, *28*, No. 1802564.

(7) Cai, Z.; Wang, J.; Lu, Z.; Zhan, R.; Ou, Y.; Wang, L.; Dahbi, M.; Alami, J.; Lu, J.; Amine, K.; et al. Ultrafast Metal Electrodeposition Revealed by In Situ Optical Imaging and Theoretical Modeling towards Fast-Charging Zn Battery Chemistry. *Angew. Chem. Int. Ed.* **2022**, *134*, No. e202116560.

(8) Hao, J.; Li, X.; Zeng, X.; Li, D.; Mao, J.; Guo, Z. Deeply understanding the Zn anode behaviour and corresponding improvement strategies in different aqueous Zn-based batteries. *Energy Environ. Sci.* **2020**, *13*, 3917−3949.

(9) Zeng, X.; Hao, J.; Wang, Z.; Mao, J.; Guo, Z. Recent progress and perspectives on aqueous Zn-based rechargeable batteries with mild aqueous electrolytes. *Energy Storage Mater.* **2019**, *20*, 410−437.

(10) Huang, J.; Guo, Z.; Ma, Y.; Bin, D.; Wang, Y.; Xia, Y. Recent Progress of Rechargeable Batteries Using Mild Aqueous Electrolytes. *Small Methods* **2019**, *3*, No. 1800272.

(11) Wang, J.; Zhang, B.; Cai, Z.; Zhan, R.; Wang, W.; Fu, L.; Wan, M.; Xiao, R.; Ou, Y.; Wang, L.; et al. Stable interphase chemistry of textured Zn anode for rechargeable aqueous batteries. *Sci. Bull.* **2022**, *67*, 716−724.

(12) Ou, Y.; Cai, Z.; Wang, J.; Zhan, R.; Liu, S.; Lu, Z.; Sun, Y. Reversible aqueous Zn battery anode enabled by a stable complexation adsorbent interface. *EcoMat* **2022**, *4*, No. e12167.

(13) Liu, H.; Li, J.; Zhang, X.; Liu, X.; Yan, Y.; Chen, F.; Zhang, G.; Duan. Ultrathin and Ultralight Zn Micromesh-Induced Spatial-Selection Deposition for Flexible High-Specific-Energy Zn-Ion Batteries. *Adv. Funct. Mater.* **2021**, *31*, No. 2106550.

(14) Han, M.; Huang, J.; Xie, X.; Li, T. C.; Huang, J.; Liang, S.; Zhou, J.; Fan, H. J. Hydrated Eutectic Electrolyte with Ligand-Oriented Solvation Shell to Boost the Stability of Zinc Battery. *Adv. Funct. Mater.* **2022**, *32*, No. 2110957.

(15) Wang, Y.; Guo, T.; Yin, J.; Tian, Z.; Ma, Y.; Liu, Z.; Zhu, Y.; Alshareef, H. N. Controlled Deposition of Zinc-Metal Anodes via Selectively Polarized Ferroelectric Polymers. *Adv. Mater.* **2022**, *34*, No. e2106937.

(16) Chen, P.; Yuan, X.; Xia, Y.; Zhang, Y.; Fu, L.; Liu, L.; Yu, N.; Huang, Q.; Wang, B.; Hu, X.; et al. An Artificial Polyacrylonitrile Coating Layer Confining Zinc Dendrite Growth for Highly Reversible Aqueous Zinc-Based Batteries. *Adv. Sci.* **2021**, *8*, No. e2100309.

(17) Han, J.; Euchner, H.; Kuenzel, M.; Hosseini, S. M.; Groß, A.; Varzi, A.; Passerini, S. A Thin and Uniform Fluoride-Based Artificial Interphase for the Zinc Metal Anode Enabling Reversible Zn/MnO2 Batteries. *ACS Energy Lett.* **2021**, *6*, 3063−3071.

(18) Zhang, Q.; Su, Y.; Shi, Z.; Yang, X.; Sun, J. Artificial Interphase Layer for Stabilized Zn Anodes: Progress and Prospects. *Small* **2022**, *18*, No. e2203583.

(19) Xiong, P.; Zhang, Y.; Zhang, J.; Baek, S. H.; Zeng, L.; Yao, Y.; Park, H. S. Recent progress of artificial interfacial layers in aqueous Zn metal batteries. *EnergyChem* **2022**, *4*, No. 100076.

(20) Wang, Y.; Liu, Y.; Wang, H.; Dou, S.; Gan, W.; Ci, L.; Huang, Y.; Yuan, Q. MOF-based Ionic Sieve Interphase for Regulated Zn2+ Flux Toward Dendrite-Free Aqueous Zinc Ion Battery. *J. Mater. Chem. A* **2022**, *10*, 4366−4375.

(21) Zhao, R.; Yang, Y.; Liu, G.; Zhu, R.; Huang, J.; Chen, Z.; Gao, Z.; Chen, X.; Qie, L. Redirected Zn Electrodeposition by an Anti-Corrosion Elastic Constraint for Highly Reversible Zn Anodes. *Adv. Funct. Mater.* **2021**, *31*, No. 2001867.

(22) Liu, J.; Khanam, Z.; Muchakayala, R.; Song, S. Fabrication and characterization of Zn-ion-conducting solid polymer electrolyte films based on PVdF-HFP/Zn(Tf)(2) complex system. *J. Mater. Sci. Mater. Electron.* **2020**, *31*, 6160−6173.

(23) Lorca, S.; Santos, F.; Fernandez Romero, A. J. A Review of the Use of GPEs in Zinc-Based Batteries. A Step Closer to Wearable Electronic Gadgets and Smart Textiles. *Polymers* **2020**, *12*, 2812.

(24) He, Y.; Zhang, Y.; Li, X.; Lv, Z.; Wang, X.; Liu, Z.; Huang, X. A novel ZnO-based inorganic/organic bilayer with low resistance for Li metal protection. *Energy Storage Mater.* **2018**, *14*, 392−401.

(25) Hao, J.; Li, X.; Zhang, S.; Yang, F.; Zeng, X.; Zhang, S.; Bo, G.; Wang, C.; Guo, Z. Designing Dendrite-Free Zinc Anodes for Advanced Aqueous Zinc Batteries. *Adv. Funct. Mater.* **2020**, *30*, No. 2001263.

(26) Feng, D.; Cao, F.; Hou, L.; Li, T.; Jiao, Y.; Wu, P. Immunizing Aqueous Zn Batteries against Dendrite Formation and Side Reactions at Various Temperatures via Electrolyte Additives. *Small* **2021**, *17*, No. 2103195.

(27) Varzi, A.; Raccichini, R.; Marinaro, M.; Wohlfahrt-Mehrens, M.; Passerini, S. Probing the characteristics of casein as green binder for non-aqueous electrochemical double layer capacitors' electrodes. *J. Power Sources* **2016**, *326*, 672−679.

(28) Dong, Y.; Jia, M.; Wang, Y.; Xu, J.; Liu, Y.; Jiao, L.; Zhang, N. Long-Life Zinc/Vanadium Pentoxide Battery Enabled by a Concentrated Aqueous ZnSO4 Electrolyte with Proton and Zinc Ion Co-Intercalation. *ACS Appl. Energy Mater.* **2020**, *3*, 11183−11192.

(29) Wan, F.; Zhang, L.; Dai, X.; Wang, X.; Niu, Z.; Chen, J. Aqueous rechargeable zinc/sodium vanadate batteries with enhanced performance from simultaneous insertion of dual carriers. *Nat. Commun.* **2018**, *9*, 1656.